Consciousness and Depth of Anesthesia Assessment Based on Bayesian Analysis of EEG Signals

Tai Nguyen-Ky*, *Member, IEEE*, Peng (Paul) Wen, and Yan Li, *Member, IEEE*

***Abstract*—This study applies Bayesian techniques to analyze EEG signals for the assessment of the consciousness and depth of anesthesia (DoA). This method takes the limiting large-sample normal distribution as posterior inferences to implement the Bayesian paradigm. The maximum a posterior (MAP) is applied to denoise the wavelet coefficients based on a shrinkage function. When the anesthesia states change from awake to light, moderate, and deep anesthesia, the MAP values increase gradually. Based on these changes, a new function B_{DoA} is designed to assess the DoA. The new proposed method is evaluated using anesthetized EEG recordings and BIS data from 25 patients. The Bland–Alman plot is used to verify the agreement of B_{DoA} and the popular BIS index. A correlation between B_{DoA} and BIS was measured using prediction probability P_K. In order to estimate the accuracy of DoA, the effect of sample n and variance τ on the maximum posterior probability is studied. The results show that the new index accurately estimates the patient's hypnotic states. Compared with the BIS index in some cases, the B_{DoA} index can estimate the patient's hypnotic state in the case of poor signal quality.**

***Index Terms*—Bayesian, depth of anesthesia (DoA), electroencephalogram (EEG), maximum a posterior (MAP), maximum posterior probability (MPP), wavelet transform.**

I. Introduction

ANESTHETISTS seek an early warning of a patient's level of hypnosis in real time. A number of methods have been developed over the years to detect the level of consciousness and determine the depth of anesthesia (DoA), such as clinical signs (systolic blood pressure, heart rate, sweating, and tears), spontaneous surface electromyogram, heart rate variability, the minimum alveolar concentration, lower esophageal contractility (LOC), and isolated forearm technique (IFT). However, these methods are not reliable and could not achieve the desired accuracy of anesthetic depth, as individual patients have variability and various factors, such as the degree of stimulation, pain induced by surgery and the use of concomitant analgesic drugs. It is impossible to gain a constant level of consciousness through precalculating the exact dose of anesthetics. Clinical investigations and individual cases report that some patients had been aware during the anesthesia at times when there were no abnormalities in blood pressure and heart rate [1]. LOC was not reliable for detecting of inadequate anesthesia when the primary anesthetic agent was used [2]. In the IFT method, patients were asked to move their fingers to check the level of the DoA. However, some patients could hear the commands but were unable to move the isolated arm. The incidence of movement with IFT could vary with the choice of anesthetic [3], [4].

Results from both human and animal studies demonstrate that changes in electroencephalogram (EEG) with anesthesia primarily reflect hypnotic information [5]–[8]. Several DoA monitoring devices were developed based on EEG. Currently, the BIS monitor is widely used in hospitals. Although the algorithms of these monitors are different and are not fully published, their basic principles can be described as the following. The cerebral state index is calculated using a fuzzy logic combination of four subparameters of the EEG signals in the time domain and the frequency domain [9]. The patient state index is the result of a complex computation that combines weighted quantitative EEG parameters reflecting many dimensions of brain electrical activities [10]. Entropy index monitoring is based on the acquisition and processing of raw EEG and FEMG signals by using Entropy algorithms to produce two parameters: state entropy over the frequency range of 0.8–32 Hz, and response entropy over the frequency range of 0.8–47 Hz [11]. In the Nacotrend index, numerous quantitative features were extracted from the time and the frequency domains, such as spectral parameters, entropy measures, and autoregressive parameters [12]. The BIS index is calculated from the following four parameters: 1) burst suppression ratio (BSR); 2) quazi suppression index; 3) relative β ratio; and 4) synchfastslow [13].

These monitors are widely used in clinical practice and they work satisfactorily most of the time. However, there are still some criticisms in some special cases, such as not consistent with the clinical observations [14], [15], not adequately detecting the transition between consciousness and unconsciousness [16], and not responsive to some anesthetic agents [17]. The time-domain analysis is used for the detection of epochs that represent the electrical suppression of EEG signals. However, that only happens in the case of very deep anesthesia. Therefore, these analyses could not be used for the light anesthesia state detection.

There are other developed methods for monitoring the DoA, such as wavelet transformation [18] and modified detrended moving average [19]. Recently, an adaptive time–frequency

Manuscript received June 13, 2012; revised November 5, 2012 and December 19, 2012; accepted December 20, 2012. Date of publication; date of current version. This work was supported in part by the Toowoomba Hospital Foundation, Australia. *Asterisk indicates corresponding author.*

*T. Nguyen-Ky is with the Faculty of Engineering and Surveying, Centre for Systems Biology, University of Southern Queensland, Toowoomba, Qld., 4350, Australia (e-mail: tai.nguyen@usq.edu.au).

P. Wen is with the Faculty of Engineering and Surveying, Centre for Systems Biology, University of Southern Queensland, Toowoomba, Qld., 4350, Australia (e-mail: pengwen@usq.edu.au).

Y. Li is with the Department of Mathematics and Computing, Centre for Systems Biology, University of Southern Queensland, Toowoomba, Qld., 4350, Australia (e-mail: liyan@usq.edu.au).

Digital Object Identifier 10.1109/TBME.2012.2236649

analysis method based on ensemble empirical-model decomposition was used to analyze EEG signals for estimating the DoA [20]. The spectral features of EEG signals were proposed in [21] for separating the anesthetic effects. The Isomap-based estimation was used to assess neurophysiological changes during anesthesia [22]. The Hurst exponent and the wavelet transform was applied in multiscale rescaled range analysis algorithms to measure the anesthetic drug effects on brain activity [23].

The Bayesian method was also applied to analyze the EEG signals for the DoA [24], [25]. Rezek *et al.* presented an autoregressive class of polyspectral models in the variation Bayesian framework [24]. Their results showed that the estimated higher order spectra can give a significant improvement for the DoA. The midlatency auditory evoked potentials were used to estimate the DoA by a neural network and the Bayesian rule [25].

In this paper, a statistical method is developed to estimate the DoA based on the Bayesian method. A denoising raw EEG data technique is introduced using the maximum a posterior (MAP) to compute a new Bayesian-wavelet threshold for the large sample posterior distribution. After denoising, the maximum posterior probability (MPP) is used to study the distribution of the EEG signal. A new function B_{DoA} is designed to estimate the anesthesia levels. To the best of our knowledge, this is the first time a Bayesian method is proposed for assessing the DoA based on the EEG signal.

This paper is organized as follows. In Section II, the data acquisition and a Bayesian wavelet denoising method is presented with a new threshold T_n. Section III introduces a relationship between the maximum posterior and anesthesia states. A new function B_{DoA} for monitoring the DoA is proposed in this section. The Bland–Altman method is used to test the degree of agreement between the new index B_{DoA} and the BIS method in Section IV. The experiment results are provided in Section V. The discussion and the limitations of the study are presented in Section VI. Finally, a short conclusion is drawn in Section VII.

II. Bayesian Wavelet Denoising

A. Data Acquisition

Based on the relevant ethics approvals, the EEG data were collected at the Toowoomba St. Vincent's Hospital. The formal consents were obtained from 25 adult patients (ASA I or II, age 42–76 years, weight 64–130 kg, gender 10 F/15 M). Operation types include minor orthopedics, peripheral generals, sinus, thyroid, middle ear, abdominals, chest wall, laparoscopic abdos, open abdos, lower abdos, perineal surgery, and laparoscopic bowels. Typical drug administration included earlier pharmaceuticals intravenous midazolam 0.05 mg/kg, fentanyl 1.5–3 μg/kg, or alfentanil 15–30 μg/kg. Intravenous propofol was induction 1–3 mg/kg as clinically appropriate and maintenance with inhaled sevoflurane or desflurane in oxygen-enriched air, or in 60% nitrous oxide in air. The airway was supported by endotracheal intubation or by laryngeal mask airway as indicated clinically. The timing of all intravenous dosing and significant intraoperative events as indicated by the BIS monitor clock was recorded by the attending anesthetist. In the meantime, clinical observations by the attending anesthetists during the data collection were also recorded for the comparison.

The BIS Quatro sensor was attached to the patient's forehead. Raw EEG data, BIS values, EMG, and signal quantity index (SQI) were obtained and exported to a USB drive. Raw EEG data were presented as a binary file documenting two channels of unfiltered signals. Each EEG sample was a 16-bit signed integer in units of 0.05 μV. The data were sampled at 128 times per second for each channel. **Q1**

B. Denoised Method

A noise EEG signal y_i of size n can be presented as

$$y_i = x_i + \varepsilon, i = 1, 2, ..., n \tag{1}$$

where x_i is the true EEG signal and ε represents a noise which is the sequence of independent and identically distributed random variable. In the wavelet domain, a transform of y_i has the form of

$$d = \hat{d} + \hat{\varepsilon} \tag{2}$$

where $d = Wy; \hat{d} = Wx; \hat{\varepsilon} = W\varepsilon; y = y_1, ..., y_n; x = x_1, ..., x_n$; and $\varepsilon = \varepsilon_1, ..., \varepsilon_n$.

Here, W is an orthogonal matrix, d is a noisy wavelet coefficient, $\hat{d}$ is the true coefficient, and $\hat{\varepsilon}$ is noise. Our goal is to estimate $\hat{d}$ from the noise observation d. The supposition to test is $H_0 : \hat{d} = 0$ versus $H_1 : \hat{d} \neq 0$.

A Bayesian wavelet threshold was proposed in [29]–[31]. Prior information with Bayesian estimation techniques was applied for the wavelet-based denoising. The MAP was used to estimate $\hat{d}$ from the noisy observation d. A large sample posterior distribution and approximations were presented by Press in [32]. The limiting large-sample normal distribution was adopted for posterior inferences of implementing the Bayesian paradigm. In [33], a larger posterior mode for the wavelet threshold was proposed by Cutillo *et al.* based on the MAP with the threshold

$$T = 2\sigma\sqrt{2k-1}, k > 1/2. \tag{3}$$

C. Statistic Model

For the model, the assumption is made that the wavelet coefficient d is normally distributed with the parameters μ and σ^2, and its density function $p(d|\mu, \sigma^2)$ is given by

$$p(d|\mu, \sigma^2) = \frac{1}{\sigma\sqrt{2\pi}} \exp\left\{-\frac{1}{2\sigma^2}(d-\mu)^2\right\}. \tag{4}$$

If $d \sim N(\mu, \sigma^2)$, then $E(d) = \mu$ and $V(d) = \sigma^2$. The parameter μ of the normal distribution is determined by the expected value and the parameter σ^2 by the variance of the random variable d.

Suppose we have normal observations $d|\hat{d} \sim N(\hat{d}, \sigma^2)$, where σ is known and the prior distribution for $\hat{d}$ is

$$\hat{d}|\lambda^2 \sim N(\mu, \lambda^2), \lambda^2 \sim (\lambda^2)^{-nk}, k > 0 \tag{5}$$

where λ^2 is the single unknown hyperparameter. Here, it is assumed that the parameters $\hat{d}$ are independent and identi-

cally distributed, and conditional on other parameters, such as $\hat{d} \sim N(\mu, \lambda^2)$. Consider a conjugate prior to $p(d|\hat{d})$ and $p(\hat{d}|\lambda^2)$, the hierarchical Bayes induces the following structure [32]:

$$\lambda^2 \sim p(\lambda^2), \hat{d}|\lambda^2 \sim p(\hat{d}|\lambda^2), d|\hat{d} \sim p(d|\hat{d}). \quad (6)$$

The likelihood function $l(d|\hat{d})$ is the probability of observing d being conditional on the values of $\hat{d}$. The prior distribution on $\hat{d}$ [33] is

$$p(\hat{d}) = \int p(\hat{d}|\lambda^2)p(\lambda^2)d(\lambda^2). \quad (7)$$

The posterior distribution expresses the information of d based on both the sample data and the prior information [33]

$$p(d, \hat{d}) = \int p(d|\hat{d})p(\hat{d}|\lambda^2)p(\lambda^2)d(\lambda^2). \quad (8)$$

D. New Bayesian Wavelet Threshold

The MAP estimator developed for the Gaussian case is

$$p(d, \hat{d}) \propto p(d, \hat{d}) \propto l(\hat{d}). \quad (9)$$

Here, $l(\hat{d})$ is the likelihood [33]

$$l(\hat{d}) = \mathrm{e}^{-\frac{1}{2\sigma^2}(d-\hat{d})^2}(\hat{d}-\mu)^{2\left(\frac{1}{2}-nk\right)}. \quad (10)$$

The goal here is to find the parameters $\hat{d}$ that maximize the posterior probability. The logarithm of the posterior is proportional to

$$\log\left\{p(d, \hat{d})\right\} \propto \log\left\{l(\hat{d})\right\} = L(\hat{d})$$
$$= \left\{-\frac{1}{2\sigma^2}(d-\hat{d})^2\right\} + (1-2nk)\log\left(\hat{d}-\mu\right). \quad (11)$$

Maximum posterior estimators are asymptotically equivalent to the classical maximum likelihood estimators. The eventual models of the posterior $p(d|\hat{d})$ happen when $L(\hat{d})$ maximizes. The derivative of $L(\hat{d})$ with respect to $\hat{d}$ is

$$\frac{\partial L(\hat{d})}{\partial \hat{d}} = \frac{\hat{d}^2 - (\mu+d)\hat{d} + \mu d + \sigma^2(2nk-1)}{\sigma^2(\mu-d)}. \quad (12)$$

Setting the derivative equal to 0, we obtain

$$d \geq \mu + 2\sqrt{\sigma^2(2nk-1)}. \quad (13)$$

To estimate the noise variance σ^2 from the noisy wavelet coefficients, the finest scale wavelet coefficient a_1 is used to compute a median estimator in [26]–[28] as

$$\sigma^2 = \frac{\text{median}(|a_1|)}{0.6745}. \quad (14)$$

Combining (13) and (14), a new threshold T_n is defined as

$$T_n = \log\left(\mu + 2\sqrt{\sigma^2(2nk-1)}\right) \quad (15)$$

with

$$\mu = \text{mean}(x). \quad (16)$$

The B_{DoA} function is used to compare the efficiency of two denoising thresholds which were presented in (3) and (15). The detail of B_{DoA} will be presented in the next section (see (24)).

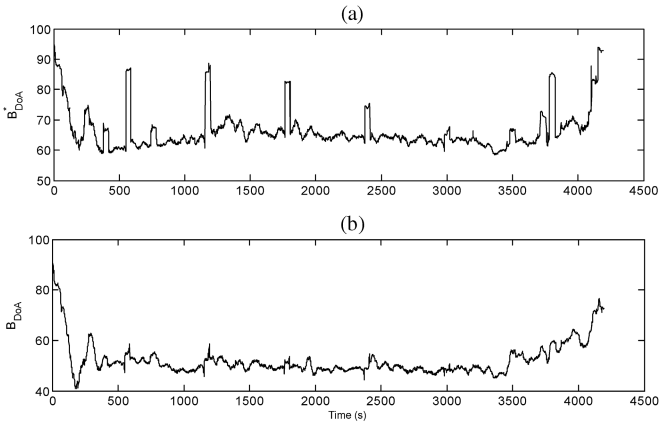

Fig. 1. Comparison between the two denoising thresholds: (a) B_{DoA} trend using the threshold in (3). (b) B_{DoA} trend using the new proposed Bayesian threshold in (15).

In Fig. 1(b), B_{DoA} clearly shows the changes of patient's states from awake state to deep anesthesia, and from general anesthesia to awake. This B_{DoA} trend used the new proposed Bayesian threshold in (25). In contrast, the trend of B_{DoA} which used the threshold in (3) has some spike noise during general anesthesia period as shown in Fig. 1(a). This indicates that our new Bayesian threshold is better than the threshold in (3) for denoising raw EEG signals.

III. Bayesian Method for the DoA

In this section, we derive the estimate method for monitoring the DoA using a Bayesian method. If the EEG signal is presented by x and denotes the set of unknown parameters by θ, the likelihood function $f(x|\theta)$ is the probability of observing the data x being conditional on the values of parameter θ. The prior distribution for θ is $\pi(\theta)$. Bayesian's theorem gives the posterior probability density function (pdf) for parameter θ as

$$f(\theta|x) = \frac{f(x|\theta)\pi(\theta)}{\int f(x|\theta)\pi(\theta)d\theta} \quad (17)$$

where f denotes the joint pdf of the data and π denotes the prior pdf of θ. If f is replaced by the likelihood function $L(\theta|x)$, we have

$$f(\theta|x) = \frac{L(x|\theta)\pi(\theta)}{\int L(x|\theta)\pi(\theta)d\theta}. \quad (18)$$

Suppose the EEG signal x has the normal observation $x|\theta \sim N(\theta, \sigma^2)$, where sigma is known and the prior distribution for θ is $\theta \sim N(\mu, \tau^2)$. We have

$$E(\theta|x) = \mu + \frac{\tau^2}{\sigma^2+\tau^2}(x-\mu) = \frac{\sigma^2\mu + \tau^2 x}{\sigma^2+\tau^2} \quad (19)$$

$$\text{Var}(\theta|x) = \frac{\tau^2\sigma^2}{\sigma^2+\tau^2}. \quad (20)$$

The posterior for θ is the normal pdf as

$$y_\theta = f(\theta|\mu, \sigma) = \frac{1}{\sigma\sqrt{2\pi}}\mathrm{e}^{-\frac{(\theta-\mu)^2}{2\sigma^2}}. \quad (21)$$

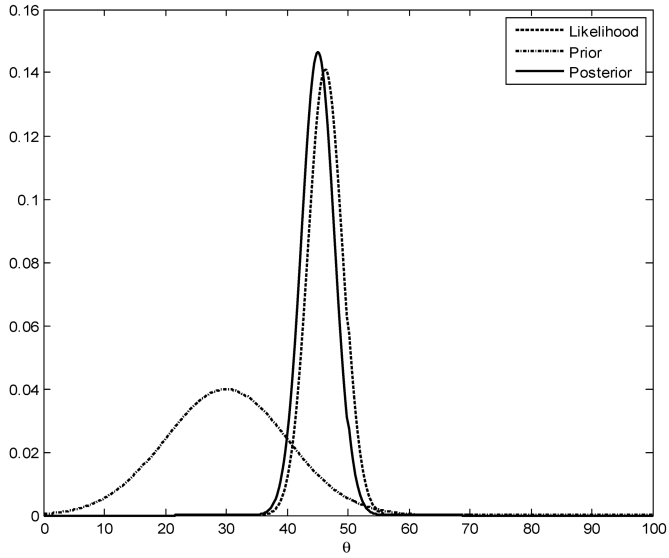

Fig. 2. Posterior, likelihood, and prior density function of the EEG signal with patient 19.

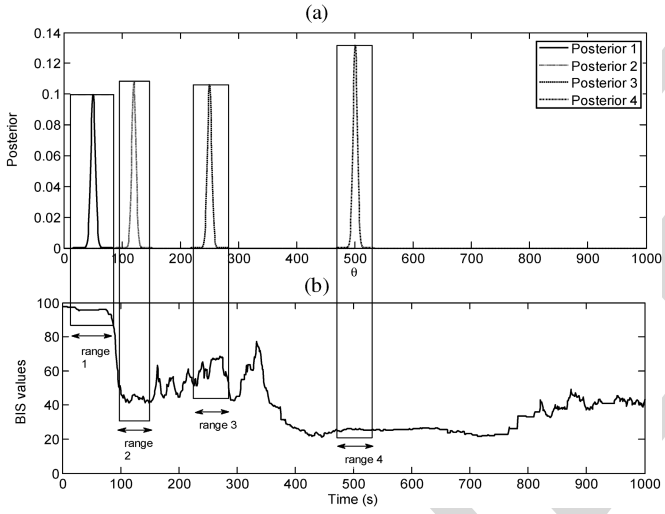

Fig. 3. Comparison between the maximum of different posterior distributions, corresponding to different anesthesia states in four sample ranges.

Fig. 2 shows the posterior, prior, and likelihood of patient's EEG data in the case of normal distributions. The posterior, likelihood and, prior density functions are shown together for the unknown parameter θ in this figure. The posterior and likelihood density functions are considerably more concentrated around their maximum values than the prior density function. A posterior density function is used to characterize the values of the parameters for the EEG data.

A. MPP of the θ Distribution

Let MPP be the maximum value of the posterior of y_θ, to give

$$\text{MPP} = \max(y_\theta). \tag{22}$$

MPP will be used to estimate the DoA. Fig. 3(a) shows four posterior graphs of y_θ in different states of anesthesia. The maximum values of the posterior in Fig. 3(a) have changed from low values to high values when the BIS trend of patient 19 changed from awake to the deep anesthesia states in Fig. 3(b). Patient 19 was a 74 yr old, 100 kg male. BIS values were recorded between 09:21:36 am and 10:33:44 am. Anesthesia induction was with intravenous midazolam 3 mg at 09:22:00, alfentanil 1000 μg at 09:22:03, and propofol 120 mg at 09:25:53. At 09:25:55, inhaled sevoflurane and nitrous oxide were introduced. The rectangles 1, 2, 3, and 4 in Fig. 3(a) cover the posteriors 1, 2, 3, and 4 which are corresponding to the ranges 1, 2, 3, and 4 in Fig. 3(b). Range 1 indicates the awake state with the BIS values from 80 to 97. Range 2 shows the moderate anesthesia state with the BIS values from 41 to 43. Range 3 represents the light anesthesia state with the BIS values from 59 to 68; while range 4 is the deep anesthesia state with the BIS values from 25 to 26.

TABLE I
RELATION BETWEEN THE ANESTHESIA STATES AND THE MPP FOR A PATIENT

Anaesthesia states	BIS value	Range	MPP
Awake	80-97	Range 1: 0-50 s	MPP_1=0.0954
Light anaesthesia	59-68	Range 3: 230-280 s	MPP_3=0.1065
Moderate anaesthesia	41-43	Range 2: 100-150 s	MPP_2=0.1083
Deep anaesthesia	25-26	Range 4: 480-530 s	MPP_4=0.1316

Table I presents a relationship between the anesthesia states and the MPP. When the anesthesia states change from awake to light, moderate, and deep anesthesia, the MPP values increase from 0.0954, 0.1065, 0.1083, and 0.1316, respectively. These changes are also shown in Fig. 3, corresponding to the four ranges in the four rectangles. These rectangles are used to connect the BIS trend and the posterior distribution in different ranges. The ranges for computing the MPP in Fig. 3 are selected, based on the levels of the anesthesia states. Each individual posterior distribution is computed within its own range and then compared on the same axis. The BIS trend shows the changes of anesthesia states over time.

B. Monitor the DoA

The MPP values have different scales for individual patients. Therefore, their values are converted to a common scale through normalization. A new scale for the MPP in the range of [0, 1] is MPP = MPP/max(MPP). Fig. 4 presents a scatter plot of the BIS and the MPP for 25 patients. The BIS values are on the x-axis in the range of [0, -100] and the MPP values are on the y-axis in the range of [0, -1]. A least-squares curve-fitting method is used to find the straight line by minimizing the distance from each point to this line. The line equation we obtained is

$$\text{MPP} = -0.0077\text{BIS} + 0.87. \tag{23}$$

This line is the best fit to a set of data points for minimizing the sum of the squared distances between the line and the data points. Based on the relation of the MPP values and the BIS values in (32) when anesthesia states change from awake to deep anesthesia, a new function is proposed to estimate the

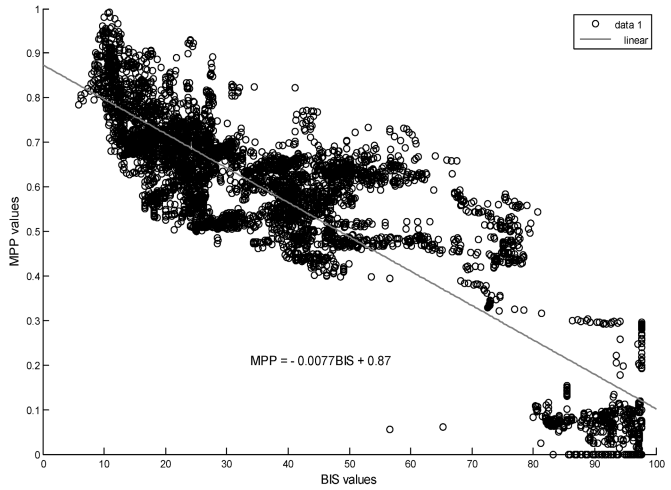

Fig. 4. Scatter plot and regression line of the BIS and MPP for 25 patients.

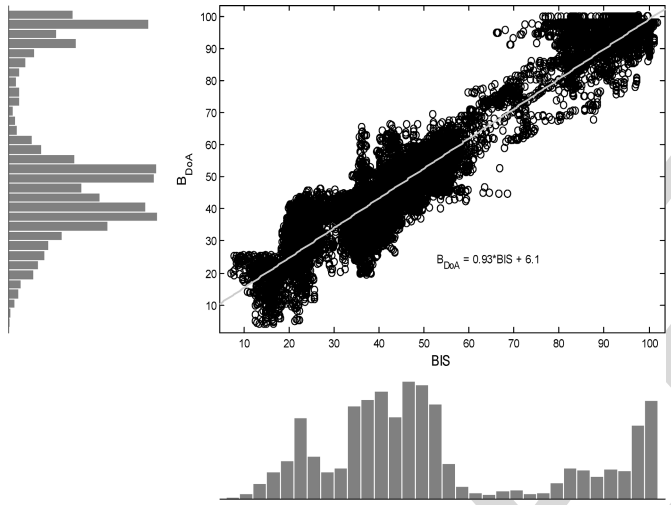

Fig. 5. Scatter plot, histograms, and regression line for the B_{DoA} and BIS values.

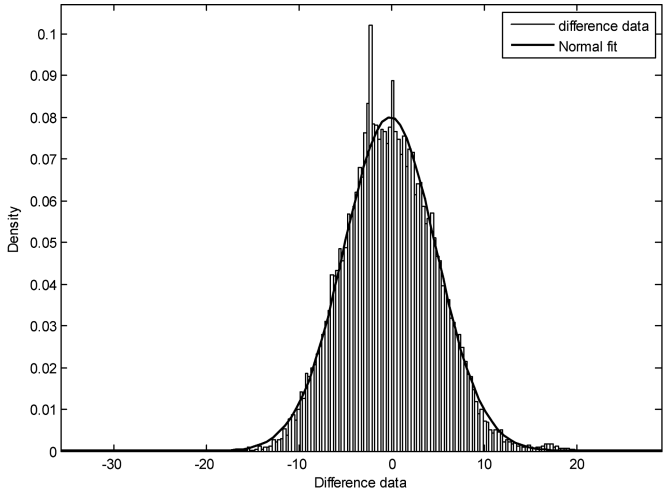

Fig. 6. Distribution of the differences (B_{DoA}–BIS) and the normal fitting.

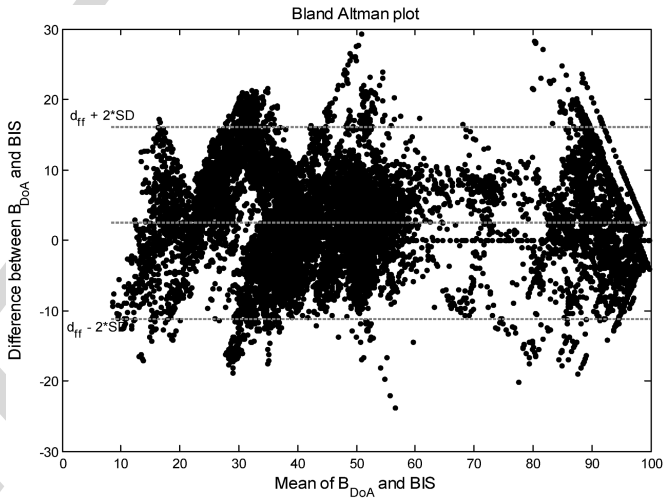

Fig. 7. Bland–Altman plot shows the difference (B_{DoA}–BIS) versus the average of values measured with 95% limits of agreement.

anesthesia levels as

$$B_{\mathrm{DoA}} = (1 - \mathrm{MPP}) \times 100 + V_{\mathrm{OFFSET}}. \tag{24}$$

Fig. 5 presents a scatter plot of the B_{DoA} and the BIS values, and their histograms on the horizontal and vertical axes. The r-squared values $r^2 = 0.9285$ and $r = 0.93$ show a strong correlation between the B_{DoA} and the BIS. The statistical significance was assumed at probability levels of $p < 0.005$.

IV. Agreement of the B_{DOA} and the BIS

To evaluate and compare our proposed method with other established methods, such as the BIS, the Bland–Altman method [36] is used to test the degree of the agreement between the proposed and BIS methods.

Defining the difference of the B_{DoA} and the BIS index as (B_{DoA}–BIS), the mean difference is $d_{\mathrm{ff}} = \mathrm{mean}(B_{\mathrm{DoA}}\text{–BIS})$, and the standard deviation of the differences is $\mathrm{SD} = \mathrm{std}(B_{\mathrm{DoA}}\text{–BIS})$. If the differences are normally distributed, 95% of the differences lie between (d_{ff} –2SD) and (d_{ff} – 2SD). The calculation of the 95% limits of agreement is based on the assumption that the differences are normally distributed. The distribution of the differences can be checked by drawing a normal plot or histogram.

Fig. 6 presents the fitting of the normal distribution of the differences (B_{DoA}—BIS). In this figure, the distribution of the differences matches well with the normal fitting. The Bland–Altman plot is presented in Fig. 7. The Bland–Altman method calculates the mean difference between two methods of the measurement (the "bias") and 95% limits of agreement as the mean difference (2SD). The Bland–Altman can include an estimation of confidence intervals for the bias and limits of agreement. In Fig. 7, there is a bias of 0.3379. The upper limit of agreement is (d_{ff} + 2SD) = 16.1, and the lower limit is (d_{ff} – 2SD) = –11.28. The 94.73% (17.500/18.473) limit of agreement presents a visual judgment of how well the two methods of the measurements agree.

Prediction probability P_K was assessed as described by Smith *et al.* [37] as a statistical test to assess the capability of a classifier to discern different levels of anesthesia. In this study, P_K is calculated using the PK tool 1.2 by Denis *et al.* [38]. A value of

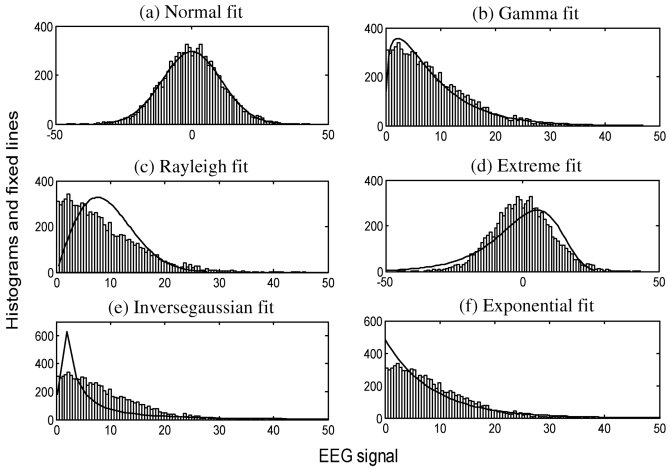

Fig. 8. EEG histogram is fitted to the different probability densities: normal, gamma, Rayleigh, extreme, inverse Gaussian, and exponential.

$P_K = 0.5$ means that the index predicts the observed state no better than 50/50 chance, and a value of $P_K = 1.0$ means that the index always predicts the observed state correctly. A value of $p < 0.05$ was considered significant. P_K was calculated for each patient. An average of these P_K (mean(P_K) $= 0.807$) preserves a good correlation between expected index values B_{DoA} and BIS.

V. Experiment Results

A. Probability Distribution of the EEG Signal

Assuming that the EEG data are the observations from a continuous probability distribution, to model the behavior of those data, the modeling will then begin by studying the distribution of the data. In practice, it is difficult to know exactly the probability distribution of the observations. A simple approach to model the behavior of the data is to form a histogram of the data. Fig. 8 plots the histogram of the EEG signal in the data vector using a number of bin bars in the histograms. The EEG histograms are fitted to the different probability densities, such as normal, gamma, Rayleigh, extreme, inverse Gaussian, and exponential. As shown in Fig. 8(a), the normal probability density model matches the histograms well. Therefore, the normal pdf is used to compute the pdf of the EEG signal.

B. Parameter Estimation

If the hyperparameters (μ and τ) are known, the posterior distribution for θ can be obtained as

$$\theta|x \sim N\left(\frac{\sigma^2\mu + \tau^2 x}{\sigma^2 + \tau^2}, \frac{\tau^2\sigma^2}{\sigma^2 + \tau^2}\right). \tag{25}$$

In practice, the situation parameters n and τ vary over time with different patients. Therefore, the B_{DoA} function may not be accurate for the large samples of patients. In order to estimate the accuracy of DoA, the effect of parameters n and τ on the MPP is studied with different values. With sample n and the sample mean $\bar{X} = 1/n \sum_{i=1}^{n} x_i$, to give

$$\theta|x_1, x_2, \ldots, x_n \sim N(\mu_p, \sigma_p) \tag{26}$$

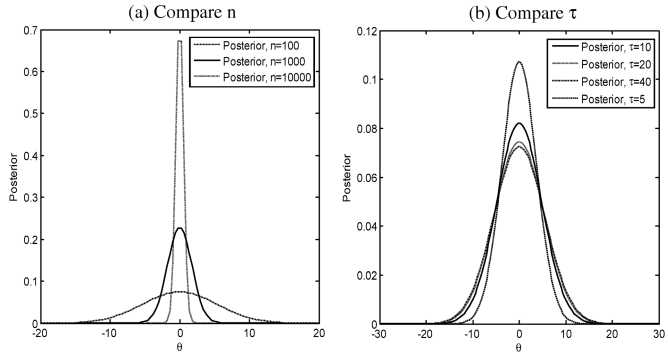

Fig. 9. Impacts of n and τ values on the posterior values. (a) MAP values increase when the sample n increases. (b) MAP values decrease when the variance τ increases.

TABLE II
B_{DoA} Values in Awake State With Different Samples (n) and Variance τ Values, BIS = 80–100

$\tau \backslash k$	1	5	10	15	20	25	30
5	91.5	89.5	87.4	85.7	84.1	82.7	81.4
10	95.0	92.1	89.5	87.5	85.7	84.1	82.7
15	95.9	92.6	89.9	87.8	86.0	84.4	83.0
20	96.3	92.8	90.1	87.9	86.1	84.5	83.1
25	96.5	92.9	90.2	88.0	86.2	84.6	83.1
30	96.7	93.0	90.2	88.0	86.2	84.6	83.1
35	96.7	93.0	90.2	88.0	86.2	84.6	83.1
40	96.8	93.1	90.2	88.1	86.2	84.6	83.1
45	96.8	93.1	90.2	88.1	86.2	84.6	83.2
50	96.8	93.1	90.3	88.1	86.2	84.6	83.2

with

$$\mu_p = \frac{\sigma^2\mu + n\tau^2\bar{X}}{\sigma^2 + n\tau^2}, \sigma_p = \frac{\tau^2\sigma^2}{\sigma^2 + n\tau^2}. \tag{27}$$

The impacts of the value of n and τ on the posterior values are shown in Fig. 9. In Fig. 9(a), when n has the values of 100, 1000, and 10000, the posteriors get the maximum values as 0.0074, 0.2263, and 0.6737, respectively. The MAP value will have a high value with a large sample n and vice versa. In Fig. 9(b), when τ has the values of 5, 10, 20, and 40, the posteriors get the maximum values as 0.1072, 0.0820, 0.0744, and 0.0724, respectively.

C. B_{DoA} Estimation Based on Bayesian Parameters

In this section, B_{DoA} values are considered based on the change of the different samples (n) and variance τ values. Four states of anesthesia are studied such as awake, light anesthesia, moderate anesthesia, and deep anesthesia states, corresponding to the BIS value ranges at 80–100, 60–80, 40–60, and 20–40, respectively. The simulation results are presented in Tables II–V. The samples (n) are chosen with the values as $n = 128 \times k$, with $k = 1, 5, 10, 15, 20, 30$. The variance τ are chosen with

TABLE III
B_{DoA} VALUES IN LIGHT ANESTHESIA STATE WITH DIFFERENT SAMPLES (n) AND VARIANCE τ VALUES, BIS = 70–80

$\tau \backslash k$	1	5	10	15	20	25	30
5	90.8	87.2	83.7	80.9	**78.4**	**76.2**	**74.1**
10	94.0	89.2	85.2	82.1	**79.5**	**77.2**	**75.1**
15	94.8	89.6	85.5	82.4	**79.7**	**77.4**	**75.2**
20	95.1	89.7	85.6	82.5	**79.8**	**77.4**	**75.3**
25	95.2	89.8	85.7	82.5	**79.8**	**77.5**	**75.3**
30	95.3	89.9	85.7	82.5	**79.9**	**77.5**	**75.4**
35	95.4	89.9	85.7	82.6	**79.9**	**77.5**	**75.4**
40	95.4	89.9	85.7	82.6	**79.9**	**77.5**	**75.4**
45	95.4	89.9	85.8	82.6	**79.9**	**77.5**	**75.4**
50	95.4	89.9	85.8	82.6	**79.9**	**77.5**	**75.4**

TABLE IV
B_{DoA} VALUES IN MODERATE ANESTHESIA STATE WITH DIFFERENT SAMPLES (n) AND VARIANCE τ VALUES, BIS = 40–55

$\tau \backslash k$	1	5	10	15	20	25	30
5	86.6	74.6	65.1	57.7	**51.4**	**45.9**	**41.0**
10	88.5	75.6	65.8	58.2	**51.9**	**46.4**	**41.4**
15	88.9	75.8	65.9	58.3	**52.0**	**46.4**	**41.5**
20	89.0	75.8	65.9	58.4	**52.0**	**46.5**	**41.5**
25	89.1	75.9	66.0	58.4	**52.0**	**46.5**	**41.5**
30	89.1	75.9	66.0	58.4	**52.1**	**46.5**	**41.5**
35	89.2	75.9	66.0	58.4	**52.1**	**46.5**	**41.5**
40	89.2	75.9	66.0	58.4	**52.1**	**46.5**	**41.5**
45	89.2	75.9	66.0	58.4	**52.1**	**46.5**	**41.5**
50	89.2	75.9	66.0	58.4	**52.1**	**46.5**	**41.5**

the values as $\tau = 5 \times m$, with $m = 1, 2, \ldots, 10$. In Table II, in awake state, the B_{DoA} values are in the range of 80–100, except the change of n and τ values. However, in Tables III and IV, the B_{DoA} values are only correct with the situations when the values n are $128 \times k$, $128 \times k$, and $128 \times k$, with $k = 20$, 25, and 30. Finally, in Table V, the B_{DoA} values are correct with the situations when the values of k are 20 and 25. Summarizing for different cases of anesthesia states, the sample n is chosen in the range of [2560, 3200], and τ values can vary from 5 to 50.

D. Choosing the θ Distribution Function

In this section, the B_{DoA} values are considered with different θ distributions, such as linear function, logarithm function, normal cumulative distribution function (cdf), and normal pdf. In order to select a best θ distribution, the B_{DoA} values are collected and compared with patient's states and the BIS values. For the linear distribution for θ [see Fig. 10(a)], the B_{DoA} trend correctly reflects the clinical changes of the patient. In Fig. 10(b),

TABLE V
B_{DoA} VALUES IN DEEP ANESTHESIA STATE WITH DIFFERENT SAMPLES (n) AND VARIANCE τ VALUES, BIS = 20–35

$\tau \backslash k$	1	5	10	15	20	25	30
5	82.6	64.6	50.7	40.1	**31.2**	**23.5**	16.5
10	84.0	65.2	51.2	40.5	**31.5**	**23.7**	16.8
15	84.3	65.3	51.2	40.5	**31.6**	**23.8**	16.8
20	84.4	65.4	51.3	40.5	**31.6**	**23.8**	16.9
25	84.4	65.4	51.3	40.6	**31.6**	**23.8**	16.9
30	84.4	65.4	51.3	40.6	**31.6**	**23.8**	16.9
35	84.5	65.4	51.3	40.6	**31.6**	**23.8**	16.9
40	84.5	65.4	51.3	40.6	**31.6**	**23.8**	16.9
45	84.5	65.4	51.3	40.6	**31.6**	**23.8**	16.9
50	84.5	65.4	51.3	40.6	**31.6**	**23.8**	16.9

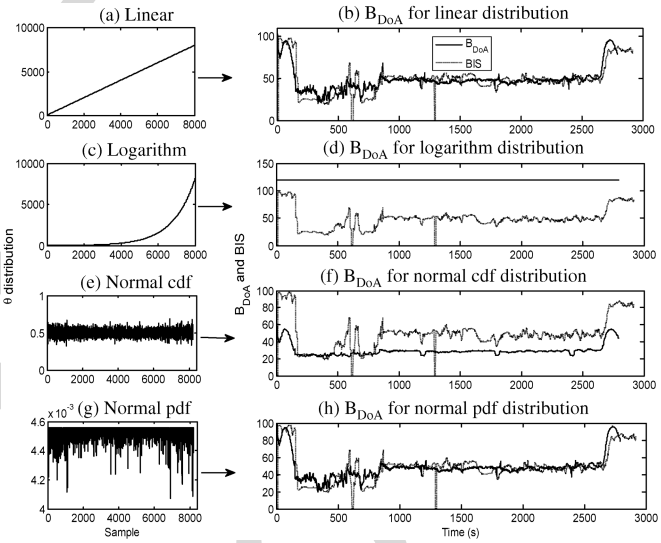

Fig. 10. Different θ distributions: linear function, logarithm function, normal CDF, and normal pdf are used to compute the B_{DoA} which were compared with the BIS trends.

the B_{DoA} trend changes from the range of 80–100 to the range of 20–40 when the patient's state changes from consciousness to unconsciousness. During the moderate anesthesia state, the B_{DoA} trend is in the range of 40–50. In the emergence state, the B_{DoA} trend increases from 50 to 95. With the logarithm distribution θ in Fig. 10(b), the B_{DoA} trend is flat as shown in Fig. 10(d). For the normal cdf in Fig. 10(c), the B_{DoA} trend in Fig. 10(f) is not close to the BIS trend.

The normal cdf is

$$\theta_{\mathrm{ncdf}} = F(x|\mu,\sigma) = \frac{1}{\sigma\sqrt{2\pi}} \int_{-\infty}^{\infty} \mathrm{e}^{-\frac{(t-\mu)^2}{2\sigma^2}} dt. \qquad (28)$$

The normal pdf is

$$\theta_{\mathrm{npdf}} = F(x|\mu,\sigma) = \frac{1}{\sigma\sqrt{2\pi}} \mathrm{e}^{-\frac{(x-\mu)^2}{2\sigma^2}}. \qquad (29)$$

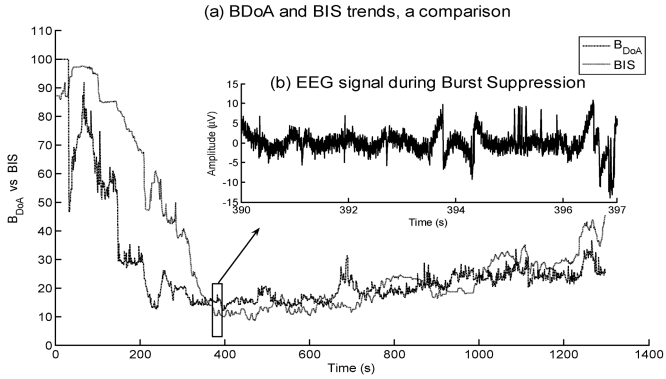

Fig. 11. Burst suppression happens from 390 to 397 s. (a) Comparison between B_{DoA} and BIS trends. B_{DoA} index can show the DoA values during the burst suppression time. (b) Sample EEG signal during the burst suppression time.

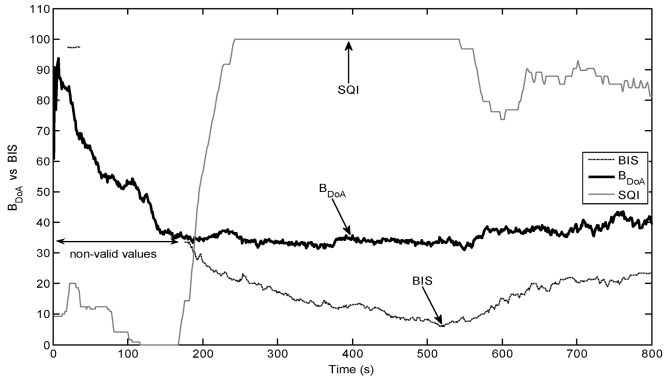

Fig. 12. DoA values in the case of poor signal quality of Patient 12: a comparison between the B_{DoA} and BIS trends. From 0 to 180 s, when SQI is lower than 15, the B_{DoA} values can display the DoA values but the BIS cannot.

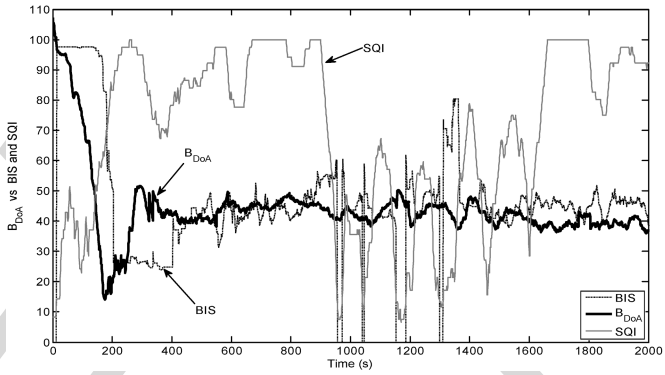

Fig. 13. During general anesthesia, the B_{DoA} values can display the DoA values but the BIS cannot when SQI is lower than 15.

For the normal pdf distribution of θ in Fig. 10(g), the B_{DoA} trend in Fig. 10(h) shows the same result as the B_{DoA} trend in Fig. 10(b). In both cases, the B_{DoA} trends are close to the BIS trends. Therefore, the linear function and the normal pdf can be chosen for the θ distribution.

E. Burst Suppression EEG Pattern

During the deep anesthesia, the EEG voltage may change from high activity to low or even isoelectricity. This pattern is known as burst suppression. The BSR is a time-domain EEG parameter developed to quantify this phenomenon (i.e., a flat EEG or no significant electrical activity in the brain). The burst suppression is recognized as those periods longer than 0.50 s, during which the EEG voltage does not exceed approximately $\pm 5.0\ \mu$V [6]. The B_{DoA} and BIS trends are shown in Fig. 11(a). This figure shows the B_{DoA} values in the range of 13.3–15.5 seconds during burst suppression, lasted 4 s from 390 to 394 s. The EEG signal during the burst suppression is shown in Fig. 11(b). During this period, the EEG signal has an amplitude value lower than 5.0 μV.

F. Patient's State in the Case of Poor Signal Quality

The BIS index is a good monitor but in some cases BIS index could not display the values on the screen when signal quality indicator (SQI) was lower than 15. This paper claims that B_{DoA} can display the DoA values in the case of poor signal quality but the BIS could not. For these cases, the BIS monitor displays a notice "Excessive artifact detected in signal". In the recorded BIS data of excel file, the value –3276.8 was labeled in these cases. In the BIS monitor, the signal quality indicator (SQI) is a measure of the signal quality for the EEG channel source and is calculated based on impedance data, artifacts, and other variables. When the signal quality is too low to accurately calculate a BIS value, the affected BIS value and other trends will not be displayed on the screen. Potential artifacts may be caused by poor skin contact (high impedance), muscle activity or rigidity, head and body motion, sustained eye movements, etc. Only "valid" BIS values are displayed on the monitor screen when signal quality index (SQI) is above 15 [22].

Fig. 12 shows a case of poor signal quality of Patient 12 when patient's state changed from awake to anesthesia. Patient 12 was a 63 yr old, 72 kg, female. Surgery was undertaken from 10:31:33 am to 10:52:26 am. Drug administration consisted of midazolam (4 mg) as a sedative drug at 10:31:35 am. At 10:31:55 am, alfentanil (1000 μg) was used as strong pain relief given only once during the operation. Parecoxib (40 mg) and Propofol (160 mg) were used at 10:32:55 am and 10:33:30 am, respectively. At 10:33:35 am, desflurane and nitrous oxide (N_2O) were started. From 0 to 180 s (10:31:33 am to 10:34:33 am), the BIS cannot display the DoA values. The clinically important transition from the awake state (BIS $= 100$) to deep anesthesia (BIS $= 33.6$) is masked by this phenomenon (see Fig. 12). In this case, the anesthetist could not use the BIS index to estimate the state of the patient.

Another case of poor signal quality is presented in Fig. 13 during general anesthesia. However, the proposed B_{DoA} index can compute and display the DoA index at times when SQI is lower than 15 and the invalid BIS value did not display on the monitor screen. The proposed B_{DoA} displays are shown in Figs. 12 and 13. Compared with the BIS index in these cases, during the periods of poor signal quality, the results of this Bayesian MMP method better correlate with clinical observations. Those other cases can be found when BIS values dropped as shown in Figs. 14 and 16(c).

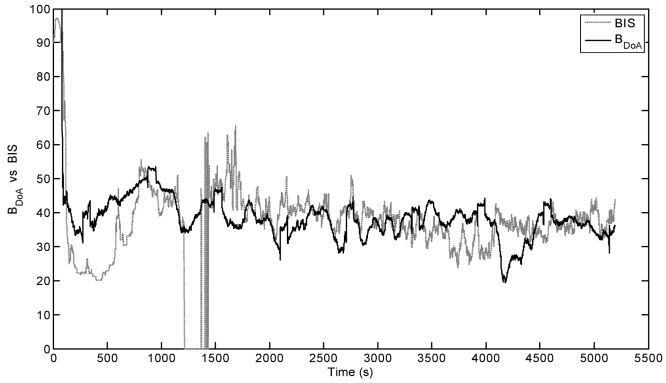

Fig. 14. Comparison between the B_{DoA} and BIS trends in the case of poor signal quality in Patient 11.

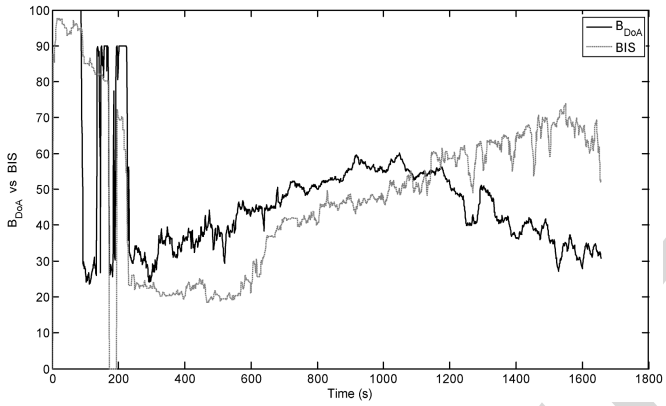

Fig. 15. Comparison between the B_{DoA} and BIS trends in the case of poor signal quality in Patient 19.

There is a case where B_{DOA} goes wrong while BIS seems to be reliable as shown in Fig. 15. At the awake state, B_{DoA} drops two times to value 25 when BIS only drops one time. At the second 1500, the BIS value increases but B_{DOA} decreases at the recovery time. In this case, probably there are impedance-related artifacts that can arise from electrode drift on the skin. In the other cases during general anesthetic, dropped B_{DoA} values do not happen but the BIS does.

G. Testing Denoise Algorithm

In order to check the denoise result, the B_{DoA} function is used for three parameters *y, x*, and ε in (1): $y = x + \varepsilon$. Here, y is a noise EEG signal, x is the EEG signal after denoising, and ε is a noise. Fig. 16(a), (b), and (c) shows the B_{DoA} of the raw EEG signal, noise, and the EEG signal after denoising, respectively. $B_{\mathrm{DoA}}(y)$ and $B_{\mathrm{DoA}}(\varepsilon)$ trends are in the range of 96.5–100 and do not have any relation to the patient's states. In contrast, $B_{\mathrm{DoA}}(x)$ trend is close to the BIS trend. This means that the denoising algorithm did not filter out any important information regarding the DoA.

VI. Discussion

In this paper, clinically observed changes in conscious state were also observed and recorded by the attending anesthetist

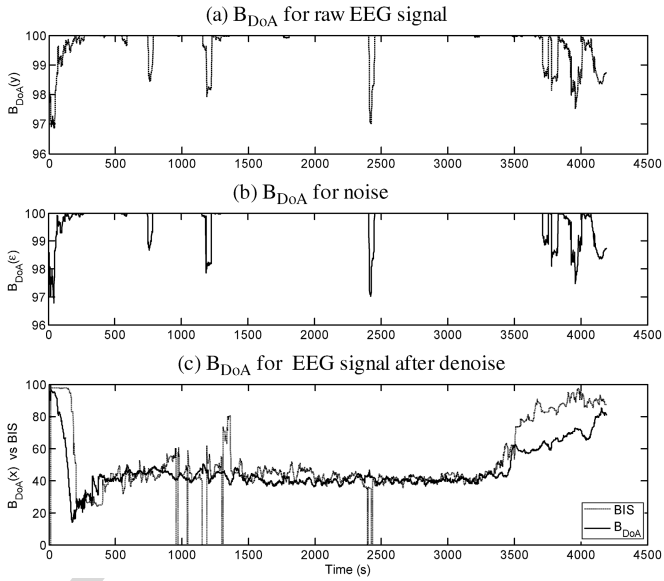

Fig. 16. (a) $B_{\mathrm{DoA}}(y)$: B_{DoA} of raw EEG signal, (b) $B_{\mathrm{DoA}}(\varepsilon)$: B_{DoA} of noise, and (c) $B_{\mathrm{DoA}}(x)$: B_{DoA} of EEG signal after denoising in Patient 4.

for comparison. The patients' responses were the overall (experienced) clinical impressions which took into account patient movement, lacrimation, heart rate, blood pressure, respiratory effort, pupil status, and, importantly, what surgery the patient had undergone. The two main components to create the anesthetic state are hypnosis created with drugs, and analgesia created with the nitrous oxide. The earlier pharmaceuticals midazolam 4 mg and alfentanil 1000 μg were induced. Most patients might not remember but might well move in response to stimuli after these drugs have been given. Loss of consciousness (LOC) occurs reliably at about 30–60 s after intravenous propofol. Assessment of LOC clinically was by lack of response to verbal and tactile stimuli. Loss of the lash reflex was used in the case of doubt. However, we did not have the plasmatic concentrations of sedative drugs. This could be a limitation of this study, especially with a small number of patients. Data exported to a USB drive and transferred to a portable computer for offline analysis. The results were compared with the BIS in the simulation, the same as with real-time analysis. Therefore, extensive testing with a larger set of subjects in real time is necessary to further improve the method. Furthermore, clinical anesthesia scales, such as the observer's assessment of anesthesia and sedation and drug concentrations, can be used as an additional reference to improve the accuracy of the DoA estimation.

VII. Conclusion

This paper studies a Bayesian method for denoising EEG signals and estimating the hypnotic DoA. First, an adaptive threshold for Bayesian wavelet denoising is proposed. The wavelet transform coefficients are modeled with prior probability distributions. A Bayesian technique is used to denoise the coefficients based on this prior information and the likelihood function. A new Bayesian threshold T_n is better than the threshold in [33] for denoising raw EEG signals.

Second, a new index B_{DoA} is proposed based on the MPP values. When the anesthesia states change from awake to light, moderate, and deep anesthesia, the MPP values increase correspondingly. The Bland–Altman method is used to test the degree of agreement between our proposed method and the BIS index. The scatterplot indicates the agreement rates of 94.73% between B_{DoA} and BIS indices. The result mean $(P_K) = 0.807$ preserves a good correlation between the expected index values B_{DoA} and BIS.

In order to estimate the accuracy of DoA, the effect of sample n and variance τ on MPP is studied. The MPP value will have the high value with a large sample n and vice versa. For different anesthesia states, the sample n is chosen in the range of [2560, 3200], and τ value can vary from 5 to 50. In order to select the best θ distributions, the B_{DoA} values are collected and compared with the patient's states and the BIS values. In the cases of the linear function and the normal pdf, the B_{DoA} trends are close to the BIS trends. Therefore, these functions are chosen for the θ distribution.

The simulation results show that the new index accurately estimates patient's hypnotic states. In addition, B_{DoA} can reflect the clinical observations better than the BIS index during the periods of poor signal quality.

ACKNOWLEDGMENT

The authors would like to express their appreciation to Dr. R. Gray, a senior anesthetist at Toowoomba Base Hospital and St. Vincent's Hospital, Australia, for his clinical knowledge and expertise in anesthesia. They would also like to thank Dr. D. Jordan and his team for supporting the PK tool 1.2.

REFERENCES

[1] N. Moerman, B. Bonke, and J. Oosting, "Awareness and recall during general anesthesia: Facts and feelings," *Anesthesiology*, vol. 79, no. 3, pp. 454–464, 1993.

[2] I. M. Schwieger, C. C. Hug, R. I. Hall, and F. S. Zlam, "Is lower esophageal contractility a reliable indicator of the adequacy of opioid anesthesia?," *J. Clin. Monit. Comput.*, vol. 5, no. 3, pp. 164–169, 1988.

[3] I. F. Russell, "Comparison of wakefulness with two anaesthetic regimens: Total IV balanced anaesthesia," *Brit. J. Anaesth.*, vol. 58, pp. 965–968, 1986.

[4] I. F. Russell, "Auditory perception under anaesthesia," *Anaesthesia*, vol. 34, p. 211, 1979.

[5] G. M. Terri, V. Saini, and B. C. Weldon, "Anesthetic management and one-year mortality after noncardiac surgery," *Anesth. Analgesia*, vol. 100, no. 1, pp. 4–10, 2005.

[6] I. J. Rampil, "A primer for EEG signal processing in anesthesia," *Anesthesiology*, vol. 89, no. 4, pp. 980–1002, 1998.

[7] J. D. Andrew, G. H. Huang, C. Czarnecki *et al.*, "Awareness during anesthesia in children: A prospective cohort study," *Anaesth. Analgesia*, vol. 100, no. 3, pp. 653–661, 2005.

[8] M. Agarwal and R. Griffiths, "Monitoring the depth of anaesthesia," *Anaesth. Intensive Care Med.*, vol. 5, no. 10, pp. 343–344, 2004.

[9] E. W. Jensen. (2005). "Cerebral state monitoring and pharmacodynamic modelling by advanced fuzzy inference—State of the art," [Online]. Available: http://www.amca2005.unibe.ch

[10] D. Drover and H. R. Ortega, "Patient state index," *Best Practice Res. Clin. Anaes.*, vol. 20, no. 1, pp. 121–128, 2006.

[11] H. Viertiö-Oja, V. Maja, and M. Särkelä, "Description of the entropy™ algorithm as applied in the datex-ohmeda s/5™ entropy module," *Acta Anaesth. Scand.*, vol. 48, no. 2, pp. 154–161, 2004.

[12] S. Kreuer and W. Wilhelm, "The narcotrend monitor," *Best Practice Res. Clin. Anaesth.*, vol. 20, no. 1, pp. 111–119, 2006.

[13] C. J. D. Pomfrett and A. J. Pearson, "EEG monitoring using bispectral analysis," *Eng. Sci. Edu. J.*, vol. 7, no. 4, pp. 155–157, 1998.

[14] R. E. Anderson, G. Barr, H. Assareh *et al.*, "Cerebral state index during anaesthetic induction: A comparative study with propofol or nitrous oxide," *Acta Anaesth. Scand.*, vol. 49, no. 6, pp. 750–753, 2005.

[15] R. E. Anderson and J. G. Jakobsson, "Cerebral state index response to incision: A clinical study in day-surgical patients," *Acta Anaesth. Scand.*, vol. 50, no. 6, pp. 749–753, 2006.

[16] G. Schneider, E. F. Kochs, B. Horn *et al.*, "Narcotrend(r) does not adequately detect the transition between awareness and unconsciousness in surgical patients," *Anesthesiology*, vol. 101, no. 5, pp. 1105–1111, 2004.

[17] G. Schneider, S. Schoniger, E. Kochs *et al.*, "Does bispectral analysis add anything but complexity? BIS sub-components may be superior to BIS for detection of awareness," *Brit. J. Anaesth.*, vol. 93, no. 4, pp. 596–597, 2004.

[18] T. Nguyen-Ky, P. P. Wen, Y. Li, and R. Gray, "Measuring and reflecting depth of anaesthesia in real-time for general anaesthesia patients," *IEEE Trans. Inf. Technol. Biomed.*, vol. 15, no. 2, pp. 630–639, Jul. 2011.

[19] T. Nguyen-Ky, P. P. Wen, and Yan Li, "An improved de-trended moving average method for accurately monitoring the depth of anaesthesia," *IEEE Trans. Biomed. Eng.*, vol. 57, no. 10, pp. 2369–2378, Oct. 2010.

[20] D. Chen, D. Li, M. Xiong, H. Bao, and X. Li, "GPGPU-aided ensemble empirical-mode decomposition for EEG analysis during anesthesia," *IEEE Trans. Inf. Technol. Biomed.*, vol. 14, no. 6, pp. 1417–1427, Nov. 2010.

[21] J. Kortelainen, E. Väyrynen, and T. Seppänen, "Depth of anesthesia during multidrug infusion: Separating the effects of propofol and remifentanil using the spectral features of EEG," *IEEE Trans. Biomed. Eng.*, vol. 58, no. 5, pp. 1216–1223, May 2011.

[22] J. Kortelainen, E. Väyrynen, and T. Seppänen, "Isomap approach to EEG-based assessment of neurophysiological changes during anesthesia," *IEEE Trans. Neural Syst. Rehabil. Eng.*, vol. 19, no. 2, pp. 113–120, Apr. 2011.

[23] Z. Liang, D. Li, G. Ouyang, Y. Wang, L. J. Voss, J. W. Sleigh, and X. Li, "Multiscale rescaled range analysis of EEG recordings in sevoflurane anesthesia," *Clin. Neurophysiol.*, vol. 123, no. 4, pp. 681–688, 2012.

[24] I. Rezek, S. J. Roberts, and R. Conradt, "Increasing the depth of anesthesia assessment," *IEEE Eng. Med. Biol. Mag.*, vol. 26, no. 2, pp. 64–73, Mar./Apr. 2007.

[25] L. Ying-Ying, J. W. Huang, and R. J. Roy, "Estimation of depth of anesthesia using the midlatency auditory evoked potentials by means of neural network based multiple classifier system," in *Proc. 19th Annu. Int. Conf. IEEE Eng. Med. Biol. Soc.*, Oct./Nov. 1997, vol. 3, pp. 1100–1103.

[26] D. L. Donoho and I. M. Johnstone, "Ideal spatial adaptation by wavelet shrinkage," *Biometrika*, vol. 81, no. 3, pp. 425–455, 1994.

[27] D. L. Donoho and I. M. Johnstone, "Adapting to unknown smoothness via wavelet shrinkage," *J. Amer. Statist. Assoc.*, vol. 90, no. 432, pp. 1200–1224, 1995.

[28] D. L. Donoho and I. M. Johnstone, "Ideal spatial adaptation via wavelet shrinkage," *Biometrika*, vol. 81, pp. 425–455, 1994.

[29] F. Abramovich, T. Sapatinas, and B. Silverman, "Wavelet thresholding via a Bayesian approach," *J. R. Statist.*, vol. 60, pp. 725–749, 1998.

[30] A. Hyvarinen, "Sparse code shrinkage: Denoising of nongaussian data by maximum likelihood estimation," *Neural Comput.*, vol. 11, pp. 1739–1768, 1999.

[31] J.-C. Pesquet and D. Leporini, "Bayesian wavelet denoising: Besov priors and non-Gaussian noises," *Signal Process.*, vol. 81, pp. 55–66, 2001.

[32] S. J. Press, *Subjective and Objective Bayesian Statistic*, 2nd ed. New York: Wiley.

[33] C. Luisa, J. Y. Young, R. Fabrizio, and V. Brani, "Larger posterior mode wavelet thresholding and applications," Georgia Inst. Technol., GA, Tech. Rep, 2005.

[34] C. P. Robert, *The Bayesian Choise*, 2nd ed. New York: Springer, 2007.

[35] K. R. Koch, *Introduction to Bayesian Statistic*, 2nd ed. New York: Springer, 2007, p. 14.

[36] J. M. Bland and D. G. Altman, "Statistical methods for assessing agreement between two methods of clinical measurement," *Lancet*, pp. 307–310, 1986.

[37] W. D. Smith and R. C. Dutton, "NT Smith: Measuring the performance of anesthetic depth indicators," *Anesthesiology*, vol. 84, pp. 38–51, 1996.

[38] D. Jordan, M. Steiner, E. F. Kochs, and G. Schneider, "A program for computing the prediction probability and the related receiver operating characteristic graph," *Anesth. Analg.*, vol. 111, no. 6, pp. 1416–1421, 2010.

Tai Nguyen-Ky (M'xx) received the B.E., M.B.A, and M.E. degrees from the Ho Chi Minh City University of Technology, Ho Chi Minh City, Vietnam, in 1991, 1999, and 2003, respectively, and the Ph.D. degree in biomedical from the University of Southern Queensland (USQ), Qld., Australia, in 2011.

He is currently a Postdoctoral Researcher at USQ. His research interests include the wireless networks, robust adaptive control, signal processing, and biomedical engineering.

Peng (Paul) Wen received the B.S. and M.S. degrees from the Huazhong University of Science and Technology, Hubei, China, and the Ph.D. degree from the Flinders University of Southern Australia, Adelaide, Australia, in 1983, 1986, and 2001, respectively.

He is a Senior Lecturer of control and computer engineering at the University of Southern Queensland, Qld., Australia. He research interests include control and instrument, modeling and simulation, artificial intelligence, and biomedical engineering.

Yan Li (M'xx) received the B.Sc. and the M.Sc. degrees from the Huazhong University of Science and Technology, Hubei, China, and the Ph.D. degree from the Flinders University of South Australia, Adelaide, Australia.

She is a Senior Lecturer in the Department of Mathematics and Computing, University of Southern Queensland, Qld., Australia. Her research interests include blind signal processing, pattern recognition, computational intelligence, and EEG research.

682 **QUERIES**

683 Q1. Author: Please check whether the acronym "SQI" is used for "signal quantity index," "signal quality indicator," "signal
684 quality index" or for all.
685 Q2. Author: Please provide the page range in Ref. [4].
686 Q3. Author: Please provide the names of all the authors in Refs. [7], [14], [16], and [17].
687 Q4. Author: Please provide the report number in Ref. [33].
688 Q5. Author: Please provide the year in which the author "Tai Nguyen-Ky" became a member of the IEEE.
689 Q6. Author: Please provide the year in which the author "Yan Li" became a member of the IEEE.